




Two-mirror aerial mapping camera design with a tilted-aplanatic secondary mirror for image motion compensation

XUEJI LIU,^{1,2}  DONGMING YUAN,^{1,2} LAIYUN SONG,^{1,2} GUOQIN YUAN,^{1,2,*} HONGWEN ZHANG,^{1,2} YALIN DING,^{1,2} AND CHANG ZHANG³

¹Changchun Institute of Optics, Fine Mechanics and Physics, Chinese Academy of Sciences, Changchun 130033, China

²Chinese Academy of Sciences, Key Laboratory of Airborne Optical Imaging and Measurement, Changchun 130033, China

³Changchun UP Optotech (Holding) Co., Ltd., Changchun 130033, China

*yuanguoqin@ciomp.ac.cn

Abstract: The optical compensation method is a promising method to compensate the image motion by driving the optical element of the system. However, the tilt motion of the optical element could induce the degradation of the image quality. Based on the Nodal Aberration Theory (NAT), this paper proposes a novel optical image motion compensation design with a secondary tilt-aplanatic two-mirror optical system (STATOS), which achieves the insensitivity on the image quality of the optical system. First, the properties of coma-free pivot point depending on the location of stop at primary mirror or secondary mirror have been analyzed respectively. Then the calculating method about construction parameters in terms of STATOS is developed. Further, the maximum tilt angle of secondary mirror could be solved using NAT under ordered specific restriction. Finally, a prototype is designed with SM-tilting result of MTF value maintain above 0.32 at the cut-off frequency of detector, where the principal distance could remain stable and the changed distortion is better than 0.03%. A test flight has been carried out to prove the desired results and feasibility of STATOS used in an aerial mapping camera.

© 2023 Optica Publishing Group under the terms of the [Optica Open Access Publishing Agreement](#)

1. Introduction

Aerial mapping camera takes wide field of view (FOV) ground-images from an airborne remote sensing platform at a high flight altitude. The high-speed relative motion between the ground-images and flight platform and the sweep motion, which was introduced by the sweeping movement during wide coverage image capture, will induce large image shift during the exposure time, resulting in image quality degradation. As a result, forward motion compensation (FMC) and sweep motion compensation (SMC) are the mandatory features for high precision aerial mapping cameras.

The FMC methods can be characterized into the following types: 1. Mechanical methods, which is carried out by shifting the detector linearly in the flight direction during exposure [1], such as DMC III digital mapping camera released by Z/I Imaging [2]. However, the mechanical method is difficult to ensure stable and reliable operation of the highly precise mechanical FMC system [3]. 2. Electronic methods, which is realized by enabling the cameras to move information during image sensor integration from one line to the next based on the sensor's CCD read out technology, which was known today as time delayed integration (TDI) [3], such as Leica ADS40/80 series mapping cameras [4,5], RCD30 camera [6]. However, in a remote TDI imaging system, it is difficult to keep the object movement relative to the sensor synchronized with the traveling of the charge packets or photo signals on the focal plane, and that the direction of the

object movement is perfectly crosswise to the rows of pixels [7,8]; 3. Optical methods, which is applied by rotating or moving a mirror or prism in optical system to change the direction of the light path to keep image still during sensor integration [9–11], such as the VISIONMAP A3-super wide angle mapping system [12,13].

In order to achieve system miniaturization and simplicity, the tilt motion of powerful mirrors such as secondary mirrors can be applied to compensate for image shift. However, tip-tilt powerful mirror (such as secondary mirror) broke the aberration balancing of coaxial optical system, where the aberration characteristics on misaligned system are expounded by many researchers. G. Catalan adopted an approximated formula to express a surface tilt induced aberration explicitly in terms of the construction parameters and ray trace quantities [14], the examples have been proposed to design reduced sensitivity to tilt or decenter of the secondary mirror in two-mirror systems [15]. M. Bottema [16,17] discussed the image quality achieved in a balloon-borne telescope by tilting the secondary mirror and also described some of the image forming properties of the tilted-aplanatic system. Subsequently, the concept of “vector multiplication” originally introduced by Shack [18], this laid the foundations of NAT. NAT was developed by Thompson [19–23] to describe the performance of aberration field in non-rotationally symmetric systems.

In recent years, several desensitization design methods [24–26] have been used to obtain an optical system with low error sensitivity based on NAT. Bauman [26] established a linear relationship among the optical surface decenter, compensator and wave aberration. Gu [24] deduced the analytical expressions of optical component manufacture and alignment errors (decenter and tilt of optical surface) and aberration introduced by those misalignments. Ma [25] derived the analytical expressions between misalignment sensitivities and optical structure parameters. While the aforementioned research most focused on eliminating the misalignment of the secondary mirror to achieve ideal alignment, little research has taken the advantage of the low sensitivity tilt secondary mirror to achieve the function of the FMC and SMC of aerial mapping camera.

In this paper, on the basis of forefather’s research, we innovatively design a two-mirror optical system of aerial mapping camera with image quality stabilized throughout tilting of secondary mirror based on the NAT. The rest of this paper is organized as follows: Section 2 gives the method to calculate the initial construction parameters of this secondary tilt-aplanatic two-mirror optical system (STATOS) for aerial mapping camera; Section 3 gives a design example of STATOS and its design process; Section 4 introduces the experimental and flight test to verify the validity and correctness of this design method proposed in section 3; At last, this paper has been concluded in section 5.

2. Initial configuration of a secondary tilted-aplanatic two-mirror optical system (STATOS)

2.1. Influence of coma-free condition on initial configuration parameters in two mirror system

For a classic two-mirror system, its initial structure mainly includes the radius (R_p, R_s), distance (d) and conic constant of the primary and secondary mirror (PM, SM). The radius (R_p, R_s) and distance (d) of PM and SM could be solved from the following expressions [27]:

$$R_p = \frac{2f}{m_2} \quad (1)$$

$$R_s = \frac{2fR_A}{1 + m_2} \quad (2)$$

$$d = \frac{(1 - R_A)f}{m_2} \quad (3)$$

where f is the effective focal length, m_2 is the magnification of SM, and R_A is the axial obstruction ratio.

Since f is generally specified by the designing requirement, the value of R_A is between 0 and 1, so m_2 value is crucial for a two-mirror system. Once m_2 is determined, only the conic constants (k_p, k_s) of PM and SM are indeterminate among the initial construction parameters.

For classical two-mirror system, k_p and k_s could be obtained according to the balance principle of third-order spherical aberration or coma. The classical Cassegrain or Gregorian form could be reached if both mirrors are independently corrected for spherical aberration; The Ritchey-Chretien form was derived from solving k_p and k_s to get both third-order spherical and coma corrected [28]. For a two-mirror system, Bottema [16] has pointed out that coma should be eliminated firstly if we want increase mirror tilt tolerances significantly. Therefore, k_p and k_s of STATOS must satisfy the coma-free conditions in NAT first.

The distance Z_{cep} between the vertex of SM and its coma-free pivot point [29] depends on the location of stop. In this paper Z_{cep}^{PM} and Z_{cep}^{SM} is used to represent the distance Z_{cep} with the stop location on PM and SM respectively. They can be expressed as the following forms [30,31]:

$$Z_{cep}^{PM} = \frac{2l(m_2 - 1)}{(m_2 + 1)(m_2 - 1 - (m_2 + 1)k_s)} \quad (4)$$

$$Z_{cep}^{SM} = \frac{2l(m_2^2 - 1)}{2m_2(m_2^2 - 1) - \frac{f}{l}m_2^3(1 + k_p)} \quad (5)$$

where l represents the back focal distance from SM vertex to system focus, the numerical relationship between system focal length f and axial obstruction ratio R_A is $l = fR_A$. When the position of stop is specified, it is possible to satisfy the coma-free condition with a known Z_{cep} and the fixed configuration parameters of a two-mirror system.

2.1.1. Stop at PM

Eq. (4) can be rewritten as following:

$$Z_{cep}^{PM} = \frac{2l}{(m_2 + 1)(1 - \frac{m_2 + 1}{m_2 - 1}k_s)} \quad (6)$$

The denominator of Eq. (6) is expressed as:

$$MZs = (m_2 + 1)(1 - \frac{m_2 + 1}{m_2 - 1}k_s) \quad (7)$$

The value of MZs varies according to m_2 at some specified values of k_s (-3,-1,0,2) representing different SM surface types, which is shown in Fig. 1. Some properties can be summarized from Fig. 1 as followed:

1. Eq. (7) has only one singularity on $m_2 = 1$. In the vicinity of this singularity, MZs value tends to infinity except for SM has a conic constant value of zero ($k_s = 0$);
2. Eq. (7) has a null point on $m_2 = -1$, which means that SM is a plane mirror, then Z_{cep}^{PM} goes to infinity, indicating that the coma-free pivot point is located at infinity. As a result, SM is obviously insensitive to lateral misalignment;
3. Eq. (7) has another null point on $k_s = (m_2 - 1) / (m_2 + 1)$, that means SM could maintain some power to make itself still insensitive to decenter misalignment at specified value of k_s ;
4. For Cassegrain form where the stop has been placed in PM, to achieve the coma-free pivot point infinitely close to SM vertex without significantly increasing the absolute value of m_2 , the only way is to choose a large value of k_s .

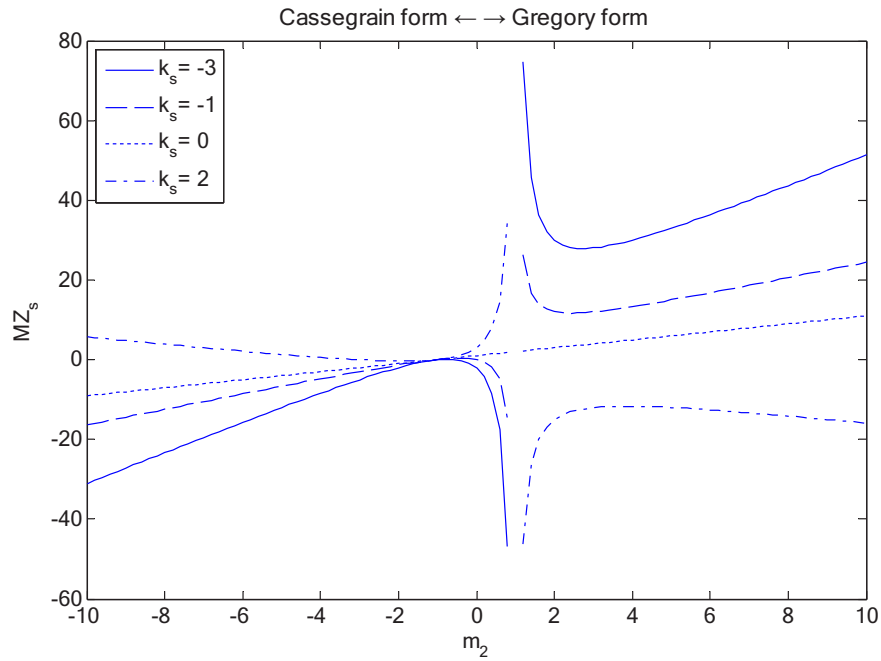


Fig. 1. Relationship between MZ_s and m_2 when SM has different surface types with the stop at PM.

2.1.2. Stop at SM

Eq. (5) can be expressed as another form:

$$Z_{cep}^{SM} = \frac{2l}{2m_2 - \frac{m_2^3}{R_A(m_2^2-1)}(1+k_p)} \tag{8}$$

The denominator can be extracted from Eq. (8) as following:

$$MZp = 2m_2 - \frac{m_2^3}{R_A(m_2^2-1)}(1+k_p) \tag{9}$$

Figure 2 illustrates the relationship between MZp and m_2 at $R_A = 0.3$ and several specific values of k_p (-3,-1,0,2) to represent different surface types of PM.

There are several conclusions obtained from Fig. 2 as followed:

1. The change rate of MZp with m_2 is faster than that of MZ_s with m_2 when k_s and k_p have the same value;
2. Eq. (9) has two singularities on $m_2 = \pm 1$, MZp tends to infinity nearby these singularities with any surface type of PM except for paraboloid ($k_p = -1$);
3. Eq. (9) has only one zero point on $m_2 = 0$, no matter what surface type of PM is, the coma-free pivot point is located at infinity and SM is insensitive to decenter misalignment;
4. For Cassegrain form with its stop at SM, m_2 value can be chosen nearby -1 to make the coma-free pivot point infinitely close to SM vertex without significantly increasing the absolute value of m_2 and k_p .

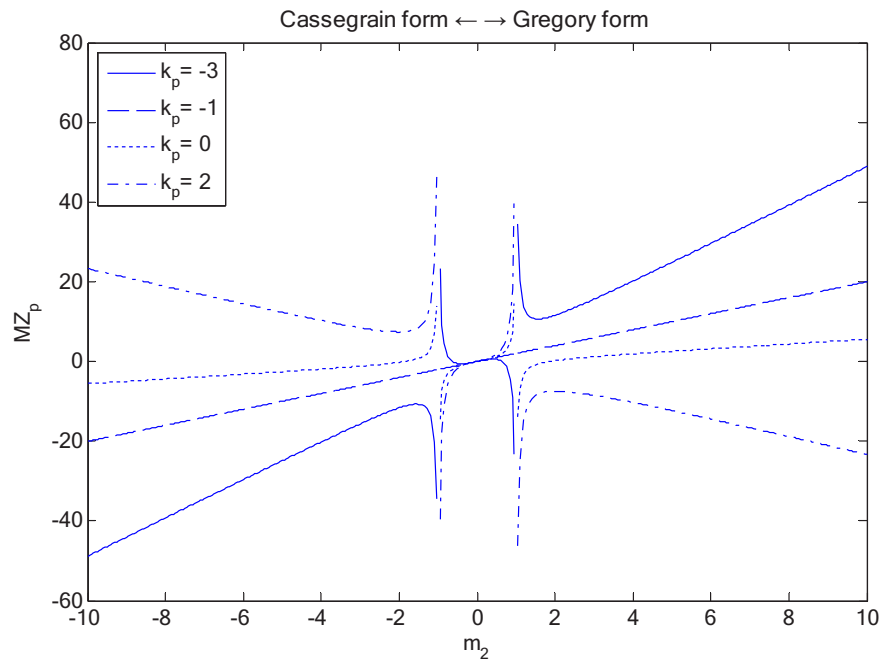


Fig. 2. Relationship between MZp and m_2 when PM has different surface types with $R_A = 0.3$ and the stop at SM.

2.2. Relationship among initial configuration parameters of STATOS

The Cassegrain form has been used widely in the aviation and spaceflight area by its compact construction, this paper mainly focuses on the Cassegrain form. To have a better control of SM, the coma-free pivot point of SM should be selected near its vertex on the focus side of PM, which means Z_{cep} goes to -0 and MZs or MZp tends to negative infinity. Meanwhile, SM should take less power to have reduced sensitivity of tilt misalignment, which leads SM to have a small value of m_2 . Under the aforementioned conditions, the stop position of STATOS needs to be set on SM. In order to reduce the aperture aberration, SM also needs a smaller m_2 , so m_2 should be chosen nearby -1 . Whether the absolute value of m_2 smaller than 1 depends on the following two factors:

Firstly, the back focal length l is constant if f and R_A are fixed. In this case, a smaller absolute value of m_2 will lead to a larger radius of curvature of PM and a longer distance between PM and SM, which may lead to a larger size optical system. Therefore, the absolute value of m_2 should be greater than 1;

Secondly, the tilt of SM is conducted to compensate the image motion. In order to obtain a larger image motion compensation angle with a smaller tilt range of SM, the larger m_2 should be selected.

Because of the above limitations, k_p needs smaller than -1 and PM has a surface type of hyperboloid, k_p value can be chosen by Z_{cep} at the specified f , R_A and m_2 . According to the classical aberration theory, the aspherical surface where the stop is located has no contribution to the off-axis aberration. As a result, the k_s value of SM can only correct the spherical aberration in STATOS. So far, it seems that the method of calculating STATOS's initial configuration parameters has been determined, and yet among the three basic constructional parameters in STATOS, the values of R_A and m_2 need to satisfy a certain range except for f is specified by

design input. The derivative of m_2 from Eq. (9) is:

$$MZ_p' = 2 - \frac{(1 + k_p)(m_2^4 - 3m_2^2)}{R_A(m_2^2 - 1)^2} \quad (10)$$

The Eq. (11) is available on $MZ_p' = 0$:

$$\frac{(1 + k_p)(m_2^4 - 3m_2^2)}{R_A(m_2^2 - 1)^2} = 2 \quad (11)$$

Since k_p smaller than -1, so $(1 + k_p) < 0$, then the range of m_2 can be solved at the condition of $(m_2^4 - 3m_2^2) < 0$ from Eq. (11) as follows: $-\sqrt{3} < m_2 < \sqrt{3}$, combination of the above conclusions, m_2 further needs to meet the following condition: $-\sqrt{3} < m_2 < -1$. For the convenience of engineering application, the focal extension Δ ($\Delta = l - |d|$) should be greater than zero, the range of R_A value could be solved from Eq. (3) with $\Delta > 0$ as followed: $R_A > -1/(m_2 - 1)$.

Next, an example is introduced to compare STATOS with the Cassegrain and Ritchey-Chretien form, which all have the same stop position on SM and the configuration parameters of $f = 1800$ mm, $m_2 = -1.3$, $R_A = 0.45$, entrance pupil diameter (EPD) = 180 mm, but their conic constants of PM and SM are different. In this classic Cassegrain form, k_p and k_s are used independently to correct spherical aberration. For the Ritchey-Chretien form, k_p and k_s are solved to get both third-order spherical and coma corrected. In STATOS, k_p is derived from a given value at $Z_{cep} = -20$ mm and k_s is used to balance spherical aberration of PM and SM. Table 1 exhibits the conic constants for the three configurations and the residual spherical (W_{040}), linear coma (W_{131}) and quadratic astigmatism (W_{222}) for the aligned state at a $\pm 0.3^\circ$ FOV. It can be seen that STATOS has larger value of residual linear coma and quadratic astigmatism on aligned state, it is necessary to introduce compensator to correct the residual aberration.

Table 1. The conic constants and wavefront coefficients of three types of two-mirror system

Types	k_p	k_s	W_{040} (Waves) ($\lambda = 0.55\mu\text{m}$)	W_{131} (Waves) ($\lambda = 0.55\mu\text{m}$)	W_{222} (Waves) ($\lambda = 0.55\mu\text{m}$)
Classic Cassegrain	-1	-58.7778	0	-0.5355	0.2492
Ritchey-Chretien	-1.9683	-233.862	0	0	0.1965
STATOS	-12.0802	-2062.3333	0	5.5925	-0.3541

The absolute values of the changed astigmatism and coma for full field from -0.3° to 0.3° are shown in Fig. 3 under the situation that SM is rotated in the meridian plane around the coma-free pivot point of STATOS at $Z_{cep} = -20$ mm by 0.1° in above three systems. The Zernike Fringe Polynomial coefficients (Z_5 and Z_8) are used to illustrate the changed astigmatism (ΔZ_5) and coma (ΔZ_8) before and after SM tilt.

It can be seen from Fig. 3 that the on-axis values of coma and astigmatism in three configurations are no longer zero since the asymmetry introduced by SM tilt. Due to the tilt around the coma-free pivot point, STATOS has the minimum changed coma of the three forms. STATOS also has a relatively small changed astigmatism among three configurations. In STATOS, the changed astigmatism is much larger than the other changed aberration, it means that the changed astigmatism has become a major limiting factor for tilt angle range of SM.

According to NAT, surface lateral misalignment (decenter or tilt) will not change the balance state of third-order spherical aberration, so the k_s value can be zero due to the existence of compensator in STATOS. It can also be conducive to optical fabrication and alignment with a spherical SM.

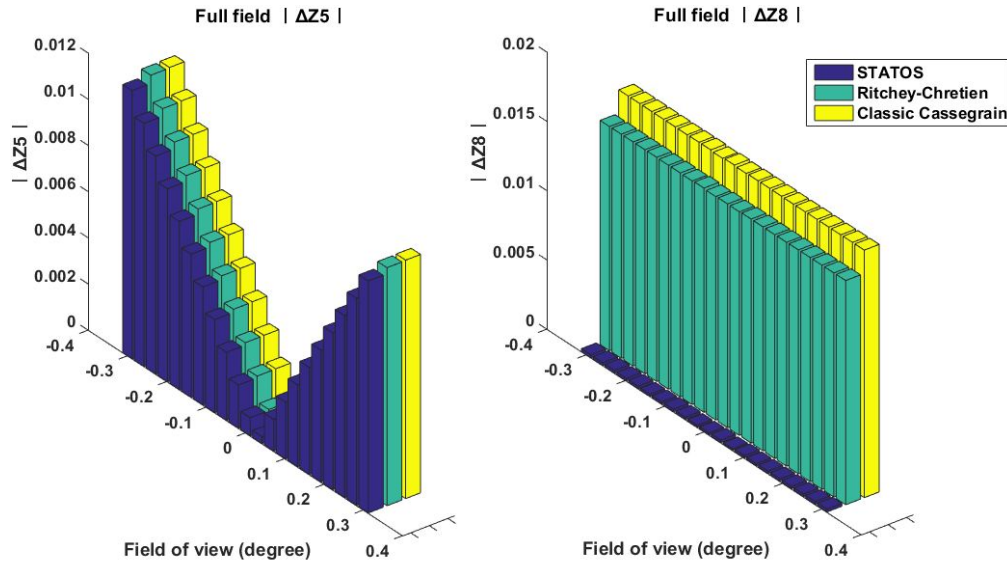


Fig. 3. The changed Fringe Zernike polynomial coefficients of Z5 and Z8 in three types two-mirror system before and after SM tilt

2.3. Maximum tilt angle of SM

It has been concluded that the changed astigmatism mainly restricts the imaging quality of STAFOS during the tilt of SM, this will limit the maximum tilt angle of SM. According to the NAT, the third-order astigmatism of a misaligned system W_{AST} can be expressed as follows:

$$W_{AST} = \frac{1}{2} \left[\left(\sum_j W_{222j} \right) \vec{H}^2 - 2\vec{H} \left(\sum_j W_{222j} \vec{\sigma}_j \right) + \left(\sum_j W_{222j} \vec{\sigma}_j^2 \right) \right] \cdot \vec{\rho}^2 \quad (12)$$

where H is the normalized field vector, ρ is the normalized pupil vector, σ_j is the introduced aberration field decenter vector of surface j .

With the assumption that STATOS can correct the inherent astigmatism with the compensator, it can be induced that $\sum_j W_{222j} = 0$, then the astigmatism introduced by SM misalignment can be expressed as:

$$\Delta W_{AST} = \frac{1}{2} [-2\vec{H}\vec{A}_{222} + \vec{B}_{222}^2] \cdot \vec{\rho}^2 \quad (13)$$

If SM is a spherical mirror, we have:

$$\begin{cases} \vec{A}_{222} = W_{222,SM}^{sph} \vec{\sigma}_{SM}^{sph} \\ \vec{B}_{222}^2 = W_{222,SM}^{sph} (\vec{\sigma}_{SM}^{sph})^2 \end{cases} \quad (14)$$

In two-mirror system, astigmatic aberration coefficient $W_{222,SM}^{sph}$ could be expressed by the structure parameters:

$$W_{222,SM}^{sph} = \frac{1}{2} \left(\frac{y_1}{f} \right)^2 \xi^0 l \left[\left(\frac{-d}{l} - \frac{EPT}{f} \right) + \frac{2f}{l(m_2 - 1)} \right]^2 \bar{u}_{PM}^2 \quad (15)$$

where y_1 is the semi-diameter of PM, \bar{u}_{PM} is the paraxial chief ray incident angle at PM, EPT is the distance of entrance pupil compared to PM, m_2 is the magnification of SM and

$$\xi^0 = \frac{(m_2 + 1)^3}{4} \left(\frac{m_2 - 1}{m_2 + 1} \right)^2 \quad (16)$$

Thompson has described in his paper [32] that the location of the center of symmetry for the spherical surface SM contribution is given by:

$$\vec{\sigma}_{SM}^{sph} = -\frac{\bar{i}^*}{\bar{i}} \quad (17)$$

where \bar{i}^* is a vector with its components defined as the angle of the optical axis ray on SM, which for a two-mirror telescope is directly the tilt perturbation of SM in the particular case, and \bar{i} denotes the paraxial angle of incidence of the chief ray at SM, which can be obtained from the paraxial ray tracing data. From the above equations, the maximum tilt angle of SM can be solved according to the restriction of maximum wave aberration ΔW_{AST} , such as Rayleigh judgment.

3. Design example of STATOS

To sum up the above conclusions, STATOS needs to balance residual spherical aberration and inherent coma aberration with a designed compensator which contains three pieces of lens. In order to reduce the aberration introduced by PM, some partial power of the entire system can be properly assigned to compensator. The flat window glass can be changed to meniscus lens in order to correct the axial chromatic aberration introduced by compensator. Code V has been chosen as the optical design software. Partial details of design results are shown in Table 2 and Table 3.

Table 2. STATOS parameters of design result

Parameters	Values
Effective photosensitive area	36 mm(H) × 23.92 mm(V)
Effective focal length	400mm
Relative aperture	f/3.7
Secondary obscuration ratio	0.5
Pixel size	7.4μm
Wave band	450~940nm
Z_{cep}	-20mm
Secondary mirror tilt angle	±0.07°
Image motion compensation angle	±0.08°

The 2D view of the designed optical system is shown in Fig. 4(a), although STATOS has a relatively long back focal length to place compensator group and imaging detector, which will lead to a larger obstruction, the impact on the quality of the image is limited on the daytime working camera.

Three cases are chosen to evaluate the performance of the system as follows:

1. SM perfectly aligned;
2. SM tilts 0.07° along detector short side direction;
3. SM tilts 0.07° along detector long side direction.

Table 3. Optical parameters for STATOS design example

Surface	Type	Conic constant	Radius	Thickness
Window glass	Sphere		587.3	16.0
	Sphere		630.5	249.0
PM	Conic	-1.8191	-836.3	-152.1
SM (stop)	Sphere		-2960.3	195.1
	Sphere		293.3	8.0
	Sphere		-112.4	3.2
Compensator	Sphere		-105.6	9.0
	Sphere		81.0	10.0
	Sphere		98.0	15.0
	Sphere		-358.9	62.4
Image	Sphere		Inf.	

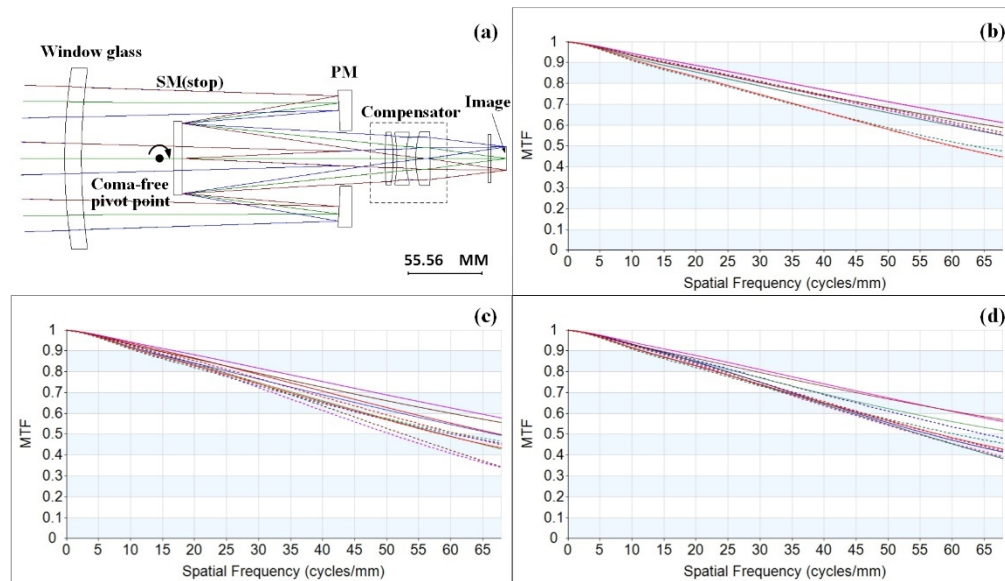


Fig. 4. the STATOS design example: (a) the 2D view layout; (b) the MTF curves with SM perfectly aligned; (c) the MTF curves with SM tilts 0.07° along detector short side direction; (d) the MTF curves with SM tilts 0.07° along detector long side direction.

The modulation transfer function (MTF) curves at above three positions named small letters (b), (c) and (d) are shown in Fig. 4. The fixed real image height at the edge of horizontal, vertical, diagonal directions from the detector central point are chosen to evaluate the image quality, the MTF values can maintain over 0.32 at cut-off frequency 68 lp/mm.

Further, it is crucial for aerial mapping camera to ensure the stability of the distortion and principal distance. The focal length of STATOS is constant by reasonable material matching and athermal design methods, so the principal distance is stable. In terms of distortion, according to the numerical simulation results of the distortion grid data in optical design software as shown in Table 4, the distortion of STATOS is better than 0.03%, which can be further depressed by calibration to ensure the mapping accuracy.

Table 4. Distortion of the STATOS design example

Relative X Field	Relative Y Field	Distortion (%)		
		Position 1	Position 2	Position 3
-1	1	0.31	0.31	0.34
0	1	0.1	0.1	0.1
1	1	0.31	0.31	0.3
-1	0	0.22	0.22	0.25
0	0	0	0	0
1	0	0.22	0.22	0.21
-1	-1	0.31	0.29	0.34
0	-1	0.1	0.08	0.1
1	-1	0.31	0.29	0.3

4. Experiments and results

In order to verify this design method of STATOS, a prototype of design example in section 3 has been made and tested, some results are depicted as follows.

4.1. Wavefront errors test in laboratory

The on-axis wavefront errors of the prototype are tested by using interferometer at wavelength 632.8 nm. As shown in Fig. 5, the on-axis root-mean-square (RMS) wavefront error value of the prototype corresponded with aligned SM is 0.047λ , which can guarantee excellent image quality. If SM has been tilted 0.07° along the long side direction of detector, the RMS value is 0.061λ , which can also maintain high imaging quality.

4.2. Dynamic target test in laboratory

In order to verify the prototype ability of image motion compensation, the dynamic target with angular velocity of $20^\circ/\text{s}$ imaging experiments is conducted in laboratory. The dynamic target comes from a collimator with a focal length of 1.6 metres, and the prototype's pixel resolution of the corresponding line pairs set number is 18. The images quality when SM compensation turned on (right) and off (left) are shown in Fig. 6. The image quality after compensation could reach the prototype's pixel resolution, the comparison between the two images illustrates that the tilt SM with fast compensate motion is effective to maintain high resolution of the image under the high relative motion between the flight platform and detector.

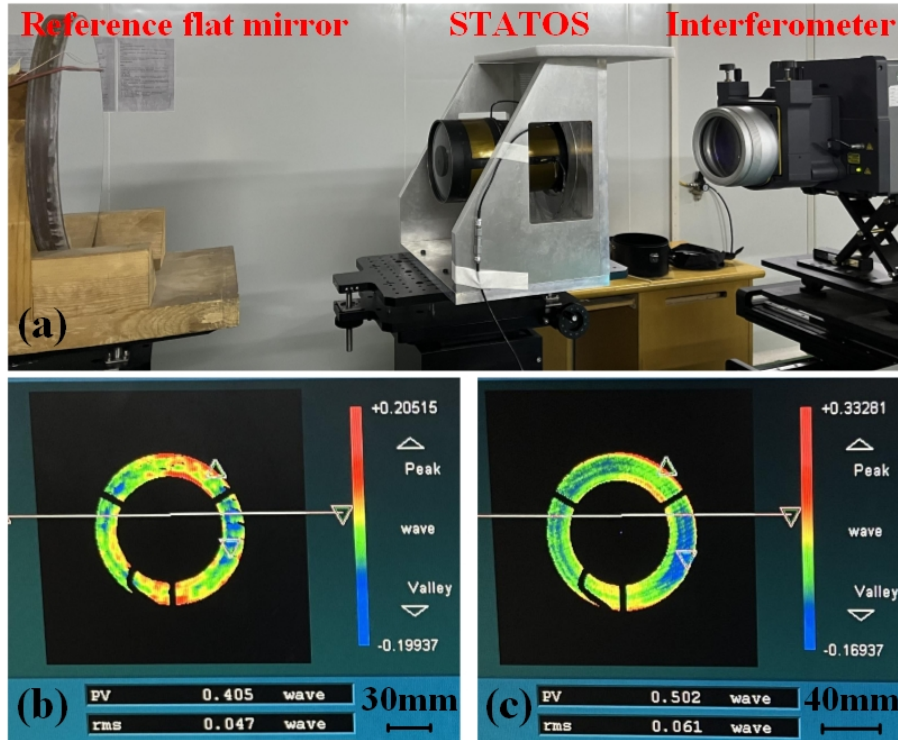


Fig. 5. Wavefront errors test of the prototype: (a) the diagrammatic sketch of test; (b) the test results with SM aligned; (c) the test results with SM tilts 0.07° along detector long side direction.

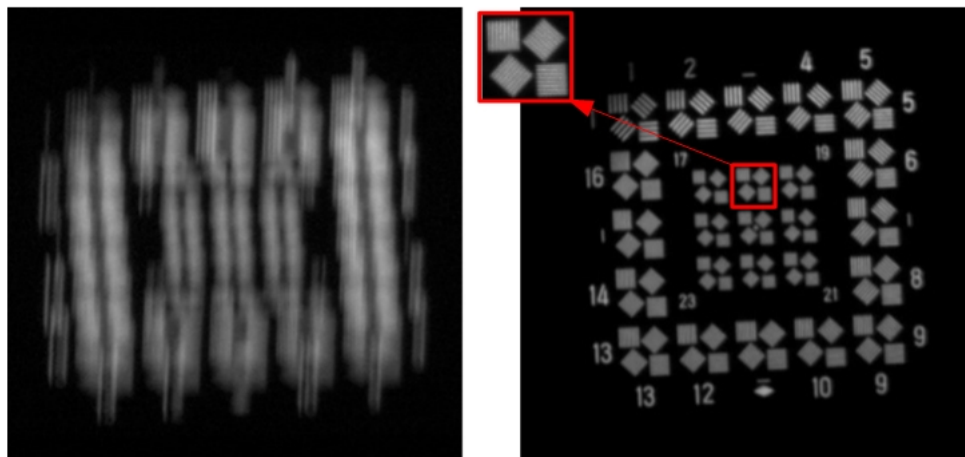


Fig. 6. Dynamic target test results of the prototype in laboratory.

4.3. Calibration results

The calibration method is carried out by using the coordinates and angles of up to 21 fixed FOV point in precise angle measurement method, the data is captured by the electronic theodolite when SM is aligned and tilted 0.07° respectively. The calibration results of the prototype are shown in Table 5.

Table 5. Calibration results of the prototype

Parameters(unit)	SM aligned	SM tilted 0.07°
principal distance(mm)	400.46	400.47
distortion on x direction(pixels)	0.07	0.08
distortion on y direction(pixels)	0.26	0.3

It can be seen from Table 5 that the principal distance is stable and the maximum distortion value is about 0.01% under the tilt motion of SM, that further proved the effectiveness of the design method of STATOS, the prototype could maintain good mapping accuracy.

4.4. flight verification

A flight test is carried out in order to verify further the prototype ability of image motion compensation in this paper. The flight altitude is about 3 km, and the maximum flight speed is nearly 300 km/h. Figure 7 shows the images before (left) and after (right) image motion compensation, the contrast ratio of the same target from Fig. 7 has been calculated and displayed in Table 6, it could be seen that the compensated imaging quality is significantly higher, and all the results could verify the validity and correctness of this design method.

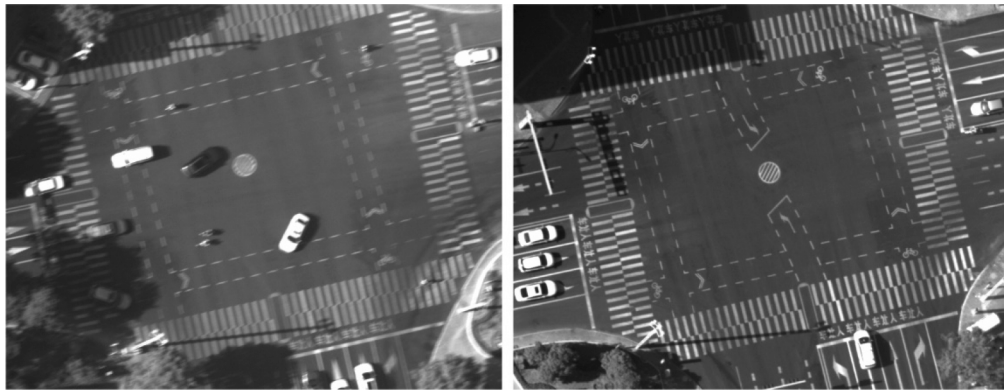


Fig. 7. Flight test images of the prototype before and after SM compensation.

Table 6. Target contrast ratio in Fig. 7

Target	Before compensation			After compensation		
	DN_max	DN_min	contrast ratio	DN_max	DN_min	contrast ratio
Sign circle in the middle of the road	203	150	0.150142	185	80	0.396226
Zebra crossing	175	150	0.076923	188	75	0.429658
White car	255	151	0.256158	255	29	0.795775

5. Conclusion

In this paper, a novel design of a two-mirror telescope with a tilt-motion SM act as motion compensation in aerial mapping camera is proposed. Based on theory of NAT, a two-mirror optical system is designed in order to obtain an insensitive SM to the misalignment of tilt and decenter. The properties of coma-free pivot point with the location of stop on PM and SM are analyzed respectively and the changed astigmatism and coma are illustrated with the tilt motion in a two-mirror system. This paper proposes a selection method on the initial configuration parameters of STATOS and the necessity for the involved compensator. With the condition that the changed astigmatism of the off-axial FOV should be satisfied with given restrictions (such as the Rayleigh criterion, etc), the maximum tilt angle of SM is given. Finally, a prototype of design has been made and tested to verify the validation of the proposed two-mirror system with the tilt-motion of the SM. The conclusion can be drawn as follows:

1. Coma should be corrected first in such optical system with rotatable SM during images capturing, since SM tilt has the most significant impact on it;
2. In a Cassegrain system, if SM tilt nearby its vertex satisfies the condition of coma-free, the stop position need be located on SM;
3. The design example results of STATOS when SM perfectly aligned and tilt 0.07° along detector long side direction respectively are as follows: a) the MTF value can maintain over 0.32 at the cut-off frequency of detector; b) the principal distance could remain stable; c) the changed distortion is better than 0.03%;
4. The experimental and flight test results show that the prototype of STATOS can effectively compensate the image motion generated by aerial mapping camera.

In the future work, the various sources of error such as manufacturing, alignment and electro-controlling impacting on the intrinsic parameters needs to be deeply analyzed.

Funding. National Natural Science Foundation of China The Young Scientists Fund (No.52105537).

Disclosures. The authors declare no conflicts of interest.

Data availability. Data underlying the results presented in this paper are not publicly available at this time but may be obtained from the authors upon reasonable request.

References

1. H. Scholer, "An FMC-equipped aerial mapping camera," *Photogrammetric Engineering and Remote Sensing* **53**, 161–165 (1987).
2. K. Neumann, M. Welzenbach, and M. Timm, "CMOS imaging sensor technology for aerial mapping cameras," in *ISPRS - International Archives of the Photogrammetry, Remote Sensing and Spatial Information Sciences*, (2016), pp. 69–72.
3. T. Tölg, G. Kemper, and D. Kalinski, "Medium format camera evaluation based on the latest phase one technology," in *ISPRS - International Archives of the Photogrammetry, Remote Sensing and Spatial Information Sciences*, (2016), pp. 121–126.
4. V. Stanojević, Z. Milonjić, D. Đorđević, S. Bakrac, M. Stojanović, and Z. Stevanovic, "Digital Surface Model Generation with Aerial Surveying System "LEICA ADS80"," (2022), pp. 107–114.
5. J. Craig, "Comparison of Leica ADS40 and Z/I imaging DMC high-resolution airborne sensors," *Proceedings of SPIE - The International Society for Optical Engineering* (2005).
6. M. Soler, W. Kornus, A. Magariños, and M. Pla, "Analyzing rcd30 oblique performance in a production environment," *ISPRS - International Archives of the Photogrammetry, Remote Sensing and Spatial Information Sciences XLI-B3*, 99–105 (2016).
7. D. Wang, T. Zhang, and H. Kuang, "Clocking smear analysis and reduction for multi phase TDI CCD in remote sensing system," *Opt. Express* **19**(6), 4868–4880 (2011).
8. H. Yu, X. Qian, M. Guo, and S. Chen, "An Antivibration Time-Delay Integration CMOS Image Sensor With Online Deblurring Algorithm," *IEEE Trans. Circuits Syst. Video Technol.* **26**(8), 1544–1554 (2016).
9. A. Lareau, "Electro-optical imaging array with motion compensation," (1992).

10. L. Fortunato, G. Colombi, A. Ondini, C. Quaranta, C. Giunti, B. Sozzi, and G. Balzarotti, "SKYWARD: the next generation airborne infrared search and track," in *Proc. SPIE*, (2016).
11. P. Vladimir, K. Yehoshua, and C. Arie, "EIOp EO/IR LOROP camera: image stabilization for dual-band whiskbroom scanning photography," in *Proc. SPIE*, (2003).
12. M. Pechatnikov, E. Shor, and Y. Raizman, "VISIONMAP a3-super wide angle mapping system basic principles and workflow," in *ISPRS Congress*, (Beijing, 2008), pp. 1735–1740.
13. M. Pechatnikov, E. Shor, and Y. Raizman, "The New Vision Map A3 Airborne Camera System," in *52nd Photogrammetric Week*, (Stuttgart, Germany, 2009), pp. 99–109.
14. G. Catalan, "Intrinsic and induced aberration sensitivity to surface tilt," *Appl. Opt.* **27**(1), 22–23 (1988).
15. G. Catalan, "Design method of an astronomical telescope with reduced sensitivity to misalignment," *Appl. Opt.* **33**(10), 1907–1915 (1994).
16. M. Bottema and R. A. Woodruff, "Image quality in telescopes with image motion compensation by secondary mirror control," *Appl. Opt.* **11**(12), 2965–2967 (1972).
17. M. Bottema and R. A. Woodruff, "Third order aberrations in cassegrain-type telescopes and coma correction in servo-stabilized images," *Appl. Opt.* **10**(2), 300–303 (1971).
18. V. R. Shack and K. Thompson, "Influence Of Alignment Errors Of A Telescope System On Its Aberration Field," *Proc. SPIE* **0251**, 146–153 (1980).
19. K. P. Thompson, *Aberration fields in tilted and decentered optical systems*, (The University of Arizona, 1980).
20. K. Thompson, "Description of the third-order optical aberrations of near-circular pupil optical systems without symmetry," *J. Opt. Soc. Am. A* **22**(7), 1389–1401 (2005).
21. K. P. Thompson, "Multinodal fifth-order optical aberrations of optical systems without rotational symmetry: spherical aberration," *J. Opt. Soc. Am. A* **26**(5), 1090–1100 (2009).
22. K. P. Thompson, "Multinodal fifth-order optical aberrations of optical systems without rotational symmetry: the comatic aberrations," *J. Opt. Soc. Am. A* **27**(6), 1490–1504 (2010).
23. K. P. Thompson, "Multinodal fifth-order optical aberrations of optical systems without rotational symmetry: the astigmatic aberrations," *J. Opt. Soc. Am. A* **28**(5), 821–836 (2011).
24. Z. Gu, Y. Wang, and C. Yan, "Optical system optimization method for as-built performance based on nodal aberration theory," *Opt. Express* **28**(6), 7928–7942 (2020).
25. H. Ma, G. Ju, and X. Zhang, "Optical design method of two-mirror astronomical telescopes with reduced misalignment sensitivities based on the nodal aberration theory," *OSA Continuum* **1**(1), 145 (2018).
26. B. J. Bauman and M. D. Schneider, "Design of optical systems that maximize as-built performance using tolerance/compensator-informed optimization," *Opt. Express* **26**(11), 13819–13840 (2018).
27. R. N. Wilson, *Reflecting Telescope Optics I*, 2 ed. (Springer, 2004), Vol. 2nd ed.
28. W. J. Smith, *Modern Optical Engineering, Fourth Edition* (SPIE, 2007), Vol. PM180, p. 768.
29. T. Schmid, K. P. Thompson, and J. P. Rolland, "A unique astigmatic nodal property in misaligned Ritchey-Chrétien telescopes with misalignment coma removed," *Opt. Express* **18**(5), 5282–5288 (2010).
30. L. C. N. Scaduto, J. Sasian, M. A. Stefani, and J. C. D. C. Neto, "Two-mirror telescope design with third-order coma insensitive to decenter misalignment," *Opt. Express* **21**(6), 6851–6865 (2013).
31. L. Noethe and S. Guisard, "Analytical expressions for field astigmatism in decentered two mirror telescopes and application to the collimation of the ESO VLT," *Astron. Astrophys., Suppl. Ser.* **144**(1), 157–167 (2000).
32. K. P. Thompson, T. Schmid, O. Cakmakci, and J. P. Rolland, "Real-ray-based method for locating individual surface aberration field centers in imaging optical systems without rotational symmetry," *J. Opt. Soc. Am. A* **26**(6), 1503–1517 (2009).